Title

Discovery and mechanistic characterization of a structurally-unique membrane active peptide

Journal

Biochimica et Biophysica Acta (BBA) - Biomembranes, 1862(10)

ISSN

0005-2736

Authors

Bansal, Shivani
Su, Wan-Chih
Budamagunta, Madhu
et al.

Publication Date

2020-10-01

DOI

10.1016/j.bbamem.2020.183394

Peer reviewed

HHS Public Access

Author manuscript

Biochim Biophys Acta Biomembr. Author manuscript; available in PMC 2021 October 01.

Published in final edited form as:

Biochim Biophys Acta Biomembr. 2020 October 01; 1862(10): 183394. doi:10.1016/j.bbamem.2020.183394.

Discovery and mechanistic characterization of a structurally-unique membrane active peptide

Shivani Bansal[†,‖], **Wan-Chih Su**[‖,§], **Madhu Budamagunta**[†], **Wenwu Xiao**[†], **Yousif Ajena**[†], **Ruiwu Liu**[†], **John C. Voss**[†], **Randy P. Carney**[§], **Atul N. Parikh**[§], **Kit S. Lam**[†,‖,*]

[†] Department of Biochemistry and Molecular Medicine, School of Medicine, University of California, Davis

[‖] Department of Chemistry, University of California, Davis

[§] Department of Biomedical Engineering, University of California, Davis

Abstract

Membrane active peptides (MAPs) have gained wide interest due to their far reaching applications in drug discovery and drug delivery. The search for new MAPs, however, has been largely skewed with bias selecting for physicochemical parameters believed to be important for membrane activity, such as alpha helicity, cationicity and hydrophobicity. Here we carry out a search-and-find strategy to screen a 100,000-membered one-bead-one-compound (OBOC) combinatorial peptide library for lead compounds, agnostic of those physicochemical constraints. Such a synthetic strategy also permits expansion of our peptide repertoire to include unnatural amino acids. Using this approach, we discovered a structurally unique lead peptide LBF14, a linear 14-mer peptide, that induces gross morphological disruption of membranes, irrespective of membrane composition. Further, we demonstrate that the unique insertion mechanism of the peptide, visualized by spinning disc confocal microscopy and further analyzed by electron paramagnetic resonance measurements, may be the cause of this large scale membrane deformation. We also demonstrate the robustness, reproducibility, and potential application of this technique to discover and characterize new membrane active peptides that display activity by local insertion and subsequent allosteric effects leading to global membrane disruption.

[*]**Corresponding Author** : Kit S Lam (KSL): kslam@ucdavis.edu.

Author Contributions

S.B., R.P.C., and K.S.L. conceived and designed the experiments. R. L. sequenced the positives hits. S.B. and W.C performed biological confirmation. S.B. and W.C.S performed microscope-based experiments, S.B. processed and compiled microscope data. S. B., J.C.V., and M.B. designed EPR and CD experiments and M.B. collected the data. S.B., J.C.V., and M.B. analyzed the EPR and CD data. S.B. composed the manuscript. All authors edited, and have given approval to the final version of the manuscript.

Declaration of interest statement

No competing financial interests have been declared.

ASSOCIATED CONTENT

Supporting Information. Supporting Information File (PDF) containing additional supporting data and supporting videos (AVI). Supporting Videos contacted time-lapse confocal microscopy images of GUVs showing fast membrane dynamics as membrane morphology is affected due to peptide.

Graphical Abstract

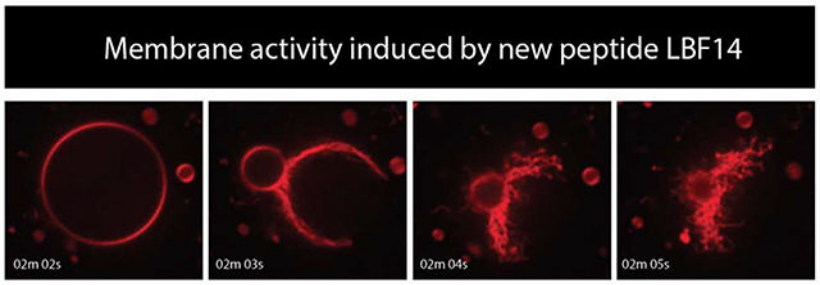

Morphological deformations demonstrated in Giant Unilamellar Vesicle, fluorescently labelled with membrane dye, caused by newly discovered membrane active peptide LBF14. These tubular deformations and subsequent disruption come form local insertion of LBF14 into the membrane which causes asymmetry in the surface areas of inner and outer bilayer.

Keywords

Combinatorial library; Membrane active peptide; Giant unilamellar vesicles; Membrane dynamics; Interfacial activity; Membrane activity

1. INTRODUCTION

Membrane active peptides (MAPs) represent a class of short peptide (< 50 AAs), with cationic (+2 to +9) and amphipathic amino acids, that display excellent membrane activity. Present in virtually all multicellular organisms[1], MAPs are an ancient component pf innate immunity. They endow the host cell with defensive antimicrobial properties[2] by selectively targeting generic featuers of many pathogenic microbial membranes via non-specific interactions[3]. Some examples include nisin(Lactococcus lactis), echinocandin. (Glarea lozoyensis), and bactitracin (Bacillus subtilis)[4]. Beyond antimicrobial varieties, some MAPs have cell-penetrating properties. These cell-penetrating peptides (CPP) can spontaneously translocate across cellular membranes and traffic biomolecular cargo intracellularly[5,6].

Beyond naturally occurring varieties, many synthetic MAPs exhibit potent membrane activity, including those selected from combinatorial library screening[7,8], engineered from natural sequences[9,10], or designed de novo[11,12]. A unifying feature of this diverse class of MAPs is that they all physically interact with cellular membranes; they bind, deform, disrupt, and permeabilize lipid bilayers. Because of these membrane remodeling capabilities, MAPs attract interest across modern biotechnology and medicine[13]. Most notably, they are being investigated as vectors for intracellular delivery of membrane-impermeable cargo, including DNA, RNA, small molecules,peptides, proteins, imaging agents, and nanoparticles[14,15]. Some MAPs may be able to discriminate between membrane compositions and compromise structural integrity of membranes of pathogens. These MAPs provide a firm foundation for developing antimicrobial, antiviral, and antifungal therapeutics that exhibit broad-spectrum efficacy, mute pathogenic drug resistance, and elicit little or no

cytolytic or cytotoxic activity against host cells [16]. Indeed, more than a thousand different MAPs have already been identified[17].

What makes MAPs membrane active? The overwhelming diversity of their sequences and conformations, together with the broad variations in modes of action, suggest that no single attribute - neither structure, nor amphiphilicity, nor charge - but rather, a unique combination of these, is key to their activity. These diverse determinants then suggest that a single MAP may exhibit multiple overlapping mechanisms of membrane interaction. Indeed, it appears that this diversity might have made it difficult for pathogens to evolve resistance against MAPs[18]. However, most MAPs derived from native proteins are generally non-selective and often toxic at the high concentrations necessary for use in vivo[19]. This calls for discovery of new and more effective MAPs. Yet current strategies like machine learning models and chemical optimization techniques[20,19] rely almost exclusively on the availability of previously-discovered MAPs, i.e. are biomimetic in nature. Therefore, these peptides that are amphipathic, a-helical, and share sequence homology with natural MAPs.

A more useful approach may be to search for new MAPs based on their general “interfacial activity,” as characterized by its ability to bind to a biomembrane, partition within the lipid/water interface, and alter the packing and organization of the bilayer, independent of peptide structure (e.g., α-helicity) or sequence (e.g., cationicity). Recent studies suggest that a MAP’s interfacial activity is a sufficient determinant of membrane activity[8,21]. From the vantage point of developing this new class of MAPs, the absence of a singular unifying mechanism for membrane interactions allows for a broader search for peptides that exhibit such interfacial activity. This approach is particularly useful for defending against pathogens known to modify properties like membrane charge in order to disrupt charge-mediated binding of MAPs, for example, cationic MAPs against gram negative bacteria[22].

To this end, the “one-bead-one-compound” (OBOC) combinatorial approach[23,24], developed in our laboratory, is well-suited for identifying new MAPs without limiting the discovery process to specific structural or sequence criteria. Specifically, the OBOC approach allows for (1) the generation of unbiased peptide libraries composed of discrete numbers of random, natural or unnatural amino acid building blocks, and (2) rapid screening for bead-bound peptides that bind to biological membranes of systematically varied molecular compositions. This high throughput, unbiased synthesis and screening methods, as demonstrated previously in our laboratory[7], allows for rapid identification of new sequences that may have no discernable homology with previously identified ones, no defined secondary structure, and no specificity in their modes of membrane interaction. Our approach parallels the previous use of combinatorial libraries[21], while expanding the repertoire of peptide building blocks to include previously unexplored unnatural amino acids that minimize susceptibility to proteolytic degradation or introduce new functionalities. In addition, we relaxed our selection criteria by selecting peptides from our 100,000-member combinatorial library that showed mere initial membrane binding using giant unilamellar vesicles (GUVs) to search for this new class of MAP, consistent with the interfacial activity model above[21].

Implementing the OBOC strategy, in conjunction with characterization of membrane activity using GUVs, we found eleven MAPs showing membrane binding regardless of specific membrane composition. Out of this pool of MAPs, we identified one in particular, LBF14, which shares no sequence, structural, or electrostatic similarity to known motifs of previously identified MAPs. By combining molecular-level characterization using electron paramagnetic resonance (EPR) spectroscopy with real-time fluorescence microscopy-based visualization of membrane remodeling at the mesoscale, we found that the interfacial activity of the MAP is not locally limited. Rather, insertion of LBF14 in the interfacial regions of the outer membrane induces local curvatures, giving rise to gross morphological remodeling that dynamically transforms vesicular membranes into dense tangles of interconnected tubules and small membrane vesicles. These findings suggest that MAPs may derive their membrane activity not only by forming local pores and localized packing distortions, but also by inducing mesoscopic morphological deformations. This strategy may pave the way for identifying an entirely new class of short MAPs, including those containing unnatural amino acids that are key to improving in vivo half-life of these peptides, and therefore their potential clinical utility as antimicrobial peptides, or vehicles to deliver payloads across targeted cell membranes of living mammalian cells.

2. MATERIALS AND METHODS

2.1 Peptide synthesis and modifications

PEGA beads (0.4mmol/g, 150–300 μm) were purchased from Agilent Technologies (Santa Clara, CA). HATU, Trifluoroacetic acid (TFA), Phenol, Rink-Amide MBHA Beads, Ammonium Acetate, Triisopropylsilane and thioanisole were purchased from Sigma Aldrich (St. Louis, MO). Ethyl Ether, Diisopropylethylamine (DIEA), Dimethylformamide (DMF), Methanol, Methylene chloride (DCM) were purchased form Fischer Scientific (Hampton, NH). 4-methylpiperidine was purchased from Spectrum (New Brunswick, NJ). Natural L-amino acids were purchased from p3BioSystems (Louisville, KY). Fmoc-Hyp-OH, Fmoc-Nva-OH, Fmoc-Dpr-OH, Fmoc-Nle-OH, Fmoc-Abu-OH were purchased from Chem Impex (Wood Dale, IL) and Fmoc-Aib-OH was purchased from ChemPep (Wellington, FL). Fmoc-Tyr(Me)-OH, Fmoc-Cha-OH and Fmoc-Orn(Boc)-OH were purchased from Ark Pharm (Arlington House, IL). Matrix-assisted laser desorption/ionization time of flight mass spectrometry (MALDI-TOF MS) analysis was performed on a Bruker UltraFlextreme mass spectrometer (Billerica, MA, USA). HPLC was performed on a Waters 2996 HPLC system equipped with a 4.6 × 150 mm Waters Xterra MS C18 5.0 μm column, and it employed a 20 min gradient from 100% aqueous H_2O (0.1% TFA) to 100% CH_3CN (0.1% TFA), at a flow rate of 1.0 mL/min. OBOC combinatorial peptide libraries were synthesized according to our previously published methods[7,23,24]. PEGA beads (2g) were washed thoroughly to duly deprotect any existing Fmoc group. Molar excess (6–7 equivalent) of each unique Fmoc-protected amino acid were added to each column of beads, along with a carbodiimide activating agent (HATU/HCTU) and a base (DIEA). The HATU/HCTU activated the carboxylic acid while the base promoted amide bond formation. The columns were shaken for 45 min at 40°C and a ninhydrin test[25] was performed on bead samples to ensure completion of reaction. If any unreacted amine group remained on the beads, the test would

appear bright blue. Following coupling, the beads were mixed together, washed copiously in fritted tube with DMF, MeOH and DCM.

The Fmoc-protecting group was then removed with 20% 4-methylpiperidine/DMF for 20 min at room temperature; a fresh solution was used during the last 5 minutes to ensure complete deprotection. These steps were then repeated for the desired length of the peptide. At the end of peptide synthesis, a global deprotection was carried out using a cocktail of 82.5% TFA, 5% phenol, water and thioanisole and 2.5% triisopropylsilane in order to cleave the acid labile groups protecting the side chains of amino acid. This step would also cleave the peptide from the bead. The acid cocktail was then added to peptides and shaken at room temperature for 4–6 hours depending on individual amino acids. In case of global deprotection, the solution was drained and neutralized with DMF and washed with MeOH and DCM. In case of cleavage from Rink resin, the solution was drained and saved in a 50ml tube as all the peptides were then in solution. Excess TFA was evaporated and the compound was precipitated using anhydrous diethyl ether. The product was collected as a white powder, which was then purified by reverse phase HPLC and its identity was confirmed with MALDI-TOF Mass Spectrometry. For dimerization, a cysteine residue was separately coupled at the N and C termini making 2 different molecules. For each molecule after cleavage as described, a 0.1M Ammonium Acetate solution was added to facilitate oxidization of free thiol to disulfide bond. This reaction was tracked using Ellman's test[26] which is able to detect a free thiol. Once no free thiol was observed both solutions were purified and confirmed with MALDI-TOF Mass spectrometry to confirm synthesis.

2.2 OBOC library design and synthesis

A combination of standard solid-phase peptide synthesis (SPPS) using Fmoc-chemistry and OBOC combinatorial technique[23] was used to prepare 4 libraries containing millions of unique peptides of varying lengths, comprising 24 natural and unnatural amino acids. Typical "split-mix" library synthesis was carried out as follows: beads (2g) were split into 24 columns and each was treated with a unique amino acid. These sub-populations were recombined and re-split into 24 populations with the assumption that 24 previously synthesized peptides were present in each column. These were then treated with the same unique amino acid which generates 24^2 unique peptides. Using OBOC and SPPS, libraries of 4 lengths that were 8,10,12 and 14 amino acids long were synthesized, in an effort to integrate diversity in length. Diversity was introduced in amino acid residues by including unnatural amino acids which may increase overall stability *in vivo.*

2.3 OBOC library screening

For sequential screening, e.g. screening with various GUVs and solution conditions, immobilization of beads was carried out in multi-well polystyrene plates using 90% DMF in water solution to soften the plastic and effectively (but not irreversibly) fix each bead at the plate surface[7,23]. GUVs were diluted to 2 mL with buffer, added to plated beads and incubated for 30 minutes. Any non-binding GUVs were washed away. Screening was performed using a confocal laser scanning microscope (CLSM, Carl Zeiss LSM 800). GUV-binding bead-bound peptides were physically isolated by micropipette, washed, and sequenced using Edman degradation micro-sequencer. Screening of about 100,000 plated

peptides was performed in a matter of 45 minutes, which included the time of incubation and recording positive beads without any lengthy processing. Bound GUVs could be washed off and treated with another type of GUV to observe the binding of a single peptides over different conditions. This screening technique is called sequential screening

2.4 GUV Synthesis

1-palmitoyl-2-oleoyl-*sn*-glycero-3-phosphocholine (POPC), 1,2-dioleoyl-sn-glycero-3-phosphocholine (DOPC), egg sphingomyelin (egg SM), cholesterol), lissamine rhodamine B 1,2-dioleyl-*sn*-glycero-3-phosphoethanolamine (Rhodamine-B DOPE), Cholesterol (ovine) (Ch) and dehydroergosterol (erg) were acquired from Avanti Polar Lipids (Alabaster, AL). 2-NBDG (2-(N-(7-Nitrobenz-2-oxa- 1,3-diazol-4-yl)Amino)-2-Deoxyglucose) (NBD-glucose) were purchased from ThermoFisher Scientific (Eugene, OR). Sucrose was obtained from EMD Chemicals (Philadelphia, PA). Chloroform was purchased from Fisher Scientific (Fair Lawn, NJ). Ninety six well glass bottom plates were obtained from MatTek Corporation (Ashland, MA). Indium tin oxide (ITO) coated glass slides with busbars (resistance 70–100 Q) were obtained from SPI Supplies (West Chester, PA) and Grace Bio-Labs Press-to-seal silicone isolators (PSA both side, 20mm diameterxlmm depth) were obtained from Sigma Aldrich (St. Louis, MO). All chemicals were used without further purification. Giant unilamellar vesicles (GUV) were prepared using a classic electroformation protocol from Angelova and Dimitrov[27] and were prepared using processes from a previously published study[28]. Two separate stock solutions - fungal GUV and mammalian GUV - mammalian consisting of 1.5:1:1.5 ratio of DOPC, Sphingomyelin and Cholesterol with 1% Rhodamine-B-DOPE in chloroform, Fungal consisting 2:1:1.3 ratio of DOPC, dehydroergosterol and sphingomyelin. Small droplets of stock solution were spread on the conductive side of ITO-coated slides to deposit 0.2ug/well and allowed to dry under vacuum overnight[29]. The dried film was then directly hydrated with 100 mM aqueous sucrose. The solution droplet was contained using a 1 mm thick adhesive silicone isolator (~20 mm diameter). A water-tight chamber was then created by sealing the second ITO slide over the ring, ensuring that no visible air bubbles were trapped inside. Using a function generator, a 3 Vpp AC sine-wave was then applied across the two slides at 10 Hz for ~2 hr[29]. During the formation the ITO sandwich was covered with an aluminium foil to protect from light. Following the formation, a 3ml syringe was used to suck the vesicle solution out of the slides. The GUVs were either used immediately or stored in small centrifuge tubes at 4 °C and used within 36 hours of preparation.

2.5 Spinning Disk Confocal Fluorescence Microscopy

Spinning disk confocal fluorescence microscopy measurements were performed using an Intelligent Imaging Innovations Marianas Digital Microscopy Workstation (3i Denver, CO) fitted with a CSU-X1 spinning disk head (Yokogawa Musashinosh, Tokyo, Japan) and a Quantem512SC EMCCD camera (Photometrics Tucson, AZ). Fluorescence micrographs were obtained using oil immersion objectives (Zeiss Fluor 40× (NA 1.3), Zeiss Plan-Fluor 63× (NA 1.4), and Zeiss Fluor 100X (NA 1.46); Carl Zeiss Oberkochen, Germany). Samples of osmotically balanced GUVs were prepared as described in the previous section. In a typical experiment, the glass bottom 96 well plate containing osmolyte-laden solution was mounted onto the microscope, and once oiled, the objectives were raised to form a meniscus

between the cover glass and the objective. To impose osmotic gradients in real-time, GUV suspension is added to the solution in the sample chambers. Rhodamine-B DOPE (Ex/Em; 560/583) was exposed with a 50 mW 561 laser line. Alexa Fluor® 488-Dextran 10,000 (Ex/Em; 495/519), NBD-PE (Ex/Em; 460/535) and 2-NBDG (Ex/Em; 465/540) were exposed with a 50 mW 488 laser line. The images are subsequently analyzed using ImageJ (http://rsbweb.nih.gov/ij/), a public-domain software, and Slidebook digital microscopy imaging software (3i Denver, CO).

2.6 Membrane Activity studies

The required concentration of peptide in 100mM of glucose was taken in a glass bottom 96-well plate. 2–4μL of the GUV solution was added to the well and imaged for a period of time. Different sections of the well were scanned to observe a range of interactions. Vesicles that showed membrane activity were tracked over several concentration and time points with different types of target membranes. To quantify the effect of peptides on the vesicles, membrane activity was used as a marker. We observe % active vesicles, a parameter developed for this particular assay, in a well to quantify the activity of a candidate peptide. Using this technique, effect of time and concentration on activity were observed and quantified. Because 100% of the vesicles did not behave in a uniform way, the standard deviation can often be large. The effect however, was still observable. Fifteen or twenty random images in a single well were taken and the total vesicles and number of active vesicles (vesicles that showed any sign of membrane activity) were counted in each picture. This study was performed in triplicate to gauge reproducibility. Standard deviation or standard error of the mean can be plotted.

2.7 EPR measurements

MTSL was obtained from Toronto Research Chemicals (North York, ON, Canada). Lead peptides were labelled with (1-oxyl-2,2,5,5-tetramethylpyrroline-3-methyl) methanethiosulfonate (MTSL) spin label via disulfide bond chemistry as is described in Methods section 2.1. Specific residues on the peptides were replaced with cysteine to introduce a free thiol and then MTSL was coupled in 2:1 peptide:MTSL ratio for 40–60 minutes. A two-fold excess of MTSL was used in order to make sure 100% of the peptide was labelled (confirmed using Ellman's test, see methods section 2.1) and excess MTSL was removed during purification using preparative HPLC and confirmed using Thermo Electron LTQ-Orbitrap XL Hybrid which utilizes electron spray ionization mass spectrometry (Thermo Scientific, Waltham, MA). An alanine walk was performed before each replacement where each amino acid is replaced with alamne and activity of each analogue is tested with an analyte. Il the activity is retained, that position is deemed unimportant for activity and suitable for labeling. The nomenclature for spin labeled peptides is CWX where CW indicates a cysteine walk, X is the residue replaced. EPR measurements were carried out using JEOL X-band spectrometer fitted with a loop-gap resonator. MTSL Spinlabelled peptide were purified and ~7μL of 100μM spinlabelled peptide was added to a sealed Quartz capillary. The spectra were taken at room temperature from three 120 min scans, over a field range of 100G at 4mW power with modulation amplitude tuned to the optimal line width of each individual spectrum, in DI water and 100mM Glucose aqueous solution as in the confocal experiments. Power saturation measurements were obtained as previously

described[30]. The molecular accessibility of each spin-labeled side chains to Ni(II)EDDA and O_2 was calculated from the $P_{1/2}$ values using software provided by C. Altenbach.

2.8 Circular Dichroism (CD)

CD measurements of the modified peptides was carried out on 200 µl of sample (0.3mg/ml) in a low [Na] CD Buller (25mM Phosphate + 100mM NaF). The CD measurements were done on JASCO J-715 CD spectrometer. CD spectra were input into an online modelling software BeStSel[31] for quantification of secondary structure populations. The graphs were fitted using an appropriate scale factor while obtaining lowest NRMSD for the best lit curve. Different spectra were observed at the same scale factor for consistency. To perform CD studies on peptide in presence of vesicles, 2µL GUV solution was added to 200µL peptide solution, incubated for 40 minutes and the spectra were observed to investigate any changes in secondary structure on interaction with the membrane.

2.9 In vitro activity and selectivity

Saccharomyces cerevisiae strain yIB12/2 that has mutated ade2 gene was provided by Xu Bao Shi (University of California, Davis), YPD Broth and 1× DPBS were purchased from Gibco (Grant Island, NY). 96-well U-bottom plate and 96-well plate was purchased form Costar (Corning, NY). MTS reagent and PMS reagents were purchased from Sigma (St.Louis, MO). From a liquid culture of *Saccharomyces cerevisiae*, 2µL was added to 196µL of YPDA media (YPD Broth with 0.5% Adenine) in a 96-well U-bottom plate. 2µL drug, solubilized in water was added in desired concentration to the well in triplicate and incubated for 48 hours at 75rpm and 30°C. In wells where yeast was killed, the solution was observed to be turbid. In contrast, wells where yeast was not killed, a white precipitate of yeast was observed at the bottom of the well. Concentrations could be varied to lit the range of study. The hemolysis of drug was analyzed using fresh citrated blood from healthy Balb/C. The red blood cells (RBCs) were collected via centrifugation at 1000 rpm for 10 min, washed three times with PBS, and then brought to a final concentration of 2% in PBS. 180 µL of erythrocyte suspension was mixed with 20 µL different concentrations of drugs and incubated for 4 h at 37°C. The mixture was centrifuged at 1000 rpm for 5 min, and 100 µL of supernatant of samples was transferred to a 96-well plate. Free hemoglobin in the supernatant was measured by the absorbance at 540 nm using a micro-plate reader (SpectraMax M2, Molecular Devices, USA). RBC were incubated with Triton-100 (0.1%) and PBS as the positive and negative controls, respectively.

MTS assay was used to evaluate the potential cytotoxicity of drugs against normal HEK293 cells. Briefly, 3×10^3 HEK293 ceils in 100 µL media per well were seeded in 96 well tissue culture plates and analysis was performed 72 hours after treatment with different concentration of drugs by adding 10 µL per well of mixture of tetrazolium compound 3-(4,5-dimethylthiazol-2-yl)-5-(3-carboxymethoxyphenyl)-2-(4-sulfophenyl)-2H-tetrazolium (MTS) and an electron coupling reagent called phenazine methosulfate (PMS) at 20:1 for 2 hours at 37°C. The 96 well plates were read on SpectraMax M2 reader (Molecular Devices, USA) at 490 nm

3. RESULTS

3.1 Sequential screening and discovery of peptide

Four OBOC combinatorial libraries of linear peptides, with four different lengths (8, 10, 12, and 14-mers) were prepared by randomizing 16 natural plus 8 unnatural amino acids (See Methods 2.2, Table 1 and SI S1.1 Figure 1), at each position (See Methods 2.1–2.3). Up to 100,000 peptide-beads could be easily immobilized on a polystyrene plate, and then probed sequentially under a confocal microscope with a series of rhodamine-labeled giant unilamellar vesicles (GUVs) for membrane-binding property. The GUVs were prepared using single phospholipids or lipid mixtures, which mimic dominant compositions of mammalian and fungal membranes (See Methods 2.4). The threshold for positively binding beads during screening was defined as any bead that would bind GUVs with sufficient affinity that they would not be removed during subsequent washing steps. This sequential screening strategy with various GUVs has allowed us to interrogate the binding profile of each and every peptide-bead to each of the GUVs. Although the ~100,000 peptide-beads in a screening experiment represent only a small fraction of all possible permutations of the peptide libraries (<0.01%), an entirely new sequence with no discernable homology or sharing physicochemical characteristics with published sequences has been discovered. Through OBOC combinatorial library screening, eleven peptides were discovered exhibiting membrane-binding to GUVs which was a direct indication of membrane activity. One of these peptides, LBF14 (Figure 1c), bound GUVs mimicking mammalian membranes and fungal membranes promiscuously. The 14-mer linear peptide LBF14, is cationic (+5) and four of the fourteen amino acids are unnatural amino acid: two 3-cyclohexyl-L-alanine, one 4-methoxytyrosine, and one ornithine.

Since the peptide was discovered while tethered to the solid support, its conformation and membrane activity in soluble form might be slightly different. We therefore resynthesized LBF14 in soluble form and studied its effects on various biological systems with different cell membranes. LBF14 was found to be hemolytic and lyse RBC with EC_{50} at 25μM after 4 h; its MIC against yeast *(S. cerevisiae)* was 50μM after 48 h; it was cytotoxic against HEK 293 cells with IC_{50} at 25μM after 72 h. This result is consistent with the membrane-agnostic behavior of LBF14. This also proved to be a satisfactory confirmation of our lead peptide and a test of the reliability of our OBOC screening and testing process.

3.2 Confocal microscopy

To characterize peptide-membrane interactions, we monitored morphological transformations induced by peptide-binding via incubation of GUVs with the LBF14 peptide at different concentrations (1 μM - 200 μM). This mixture was imaged by spinning disc confocal fluorescence microscopy to capture dynamic interaction in real time. GUVs (20–50 μm in diameter) were prepared by standard electroformation and consisted either primarily of a single unsaturated phospholipid, namely 1-palmitoyl 2-oleoyl-sn-1-glycero-3-phospho-choline (POPC) or 1,2- dioleoyl-sn-1-glycero-3-phospho-choline (DOPC). In addition to these vesicles, a second set of GUVs were prepared to mimic prototypical compositions of mammalian plasma and fungal membranes[32], using multicomponent mixtures of DOPC, sphingomyelin, cholesterol, or ergosterol. To enable fluorescence visualization of the

membrane, we added 0.5 mol% of a fluorescent-probe conjugated lipid:1,2-dioleoyl-sn-glycero-3-phospho-ethanolamine-N-lissamine rhodamine B sulfonyl (Rho-DOPE) during the preparation of GUVs (See Methods 2.4). In each of these defined vesicle types (DOPC, POPC, fungal, mammalian), the characteristic deformation when mixed with LBF14 peptide, involves bending of the vesicular membrane. Time-lapse movies obtained with spinning disc confocal fluorescence has enabled us to characterize these membrane dynamics (Figure 2, See SI Video S2.1). Within seconds after the addition of LBF14, the initially spherical GUV surface began to exhibit undulations, likely reflecting the incorporation of the peptide within the membrane interface. These undulations quickly morphed into a large number of narrow tubules that project outward, uniformly covering the vesicular surface. Tubules continued to grow over the course of the next several seconds, causing the vesicular lumen to shrink, until the GUV was transformed or “burst” into a rapidly fluctuating bundle of tubes. The tubules in the bundle were several micrometers long, with diameters near the optical resolution, and exhibited uniform fluorescence intensity consistent with a fixed diameter. These tubule bundles further rearranged themselves into an interconnected tubular network, which did not dissociate into the solution but rather remain stable, while displaying short vibrating motions. This vesicle-to-tubular network transformation was found to be stochastic with different vesicles exhibiting different kinetics of transition.

3.3 Membrane activity

We repeated these experiments while varying peptide concentration and GUV composition. LBF14 was treated with GUVs at various concentrations ranging from 1 μM to 200 μM. This gave rise to a diversity of membrane deformations in a concentration-dependent manner. As the MAP concentration increased, the membrane dynamic effect was found to be more pronounced and aggressive, with increased tubulation on single vesicles or more vesicles showing the dynamic effect. Effects of LBF14 on four different GUVs with four different lipid-compositions appeared to be very similar. At lower concentrations (1μM), generation of small ripple-like projections in the membrane was observed (See SI Section S1.2 Figure 2). Further, outward budding of vesicles was observed to be caused by the interaction of LBF14 at higher concentrations and in some cases generation of dense tangle of elongated tubules from the surface of bilayer was observed as well (See SI Section S1.2 Figure 2). At higher concentrations, vesicles were observed to have burst and then rearranged into a stable network of tubules that did not dissipate in the solution, a phenomena we believe is initiated by quick generation of buds/tubules that may cause stress on the membrane (Figure 2).

This generation of spontaneous curvature, facilitated by the new MAP LBF14, could be a direct consequence of the following effects: (1) difference in chemical composition of the outer and inner leaflet of the bilayers (2) difference in concentration of external and internal milieu generating an osmotic pressure, and/or (3) difference in area of outer and inner leaflet of bilayers. In our experimental system, given that GUV composition is locally homogenous and that the intravesical and extravesical sucrose solution concentrations (See Methods 2.4) are the same, we reason that the interfacial activity of the LBF14 peptide at the membrane/water interface causes it to insert into the outer membrane leaflets totally or partially,

resulting in an asymmetry in area between the inner and outer bilayer leaflets. This area asymmetry manifests morphologically through the emergence of tubules, as a stabilizing effect. As the local concentration of peptide increases, the tubulation/budding phenomena also increases, causing a cascade of membrane stress resulting in the observed structural disintegration of the membrane (Sequence represented in Figure 3). Essentially, the membrane compensates for the energy penalty of peptide insertion by bulging outward.

To support this hypothesis, we investigated the molecular behavior of individual amino acid residue with respect to the biological membrane, using a more mechanistically appropriate tool, electron paramagnetic resonance (EPR) spectroscopy.

3.4 Mechanistic confirmation

To explore the molecular environment around peptide LBF14, we labeled certain amino acid positions with a spin label, a molecule containing an unpaired electron. Under applied magnetic field, spin labels provide detailed information regarding their molecular environment. This type of experiment can be used in a systematic way to define the local environment, e.g., whether the moiety is inserted in the hydrophobic core of the membrane, and to what extent. To do this, every second or third amino acid was replaced in turn with cysteine. This enabled us to load a thiolated MTSL spin label to those positions via disulfide linkage. Thus, we generated six peptide analogues with spin labels at various positions (See Methods 2.7 and SI Section S1.3 Figure 4). Since this was akin to a cysteine walk, the nomenclature of the peptide was assigned as CW-X where X was the position of amino acid replaced. To observe how the local environment of each position was affected upon interaction with the membrane, the collisional frequency of diffusible relaxers was measured by power saturation EPR on the spin-labeled peptide analogues with and without GUVs (Figure 4). The changes in accessibility of the spin-label suggest positions 4, 6 and 12 were buried in the membrane upon vesicle binding, with the N- and C-terminus possibly anchored on the membrane surface. This observation is consistent with a mechanism where the peptide causes membrane disruption by lodging itself in the outer bilayer leaflet of the membrane and triggering a generation of curvature. This is also consistent with the continuous wave EPR spectra (at room temperature) for each analogue represented in SI Section S1.6, Figure 6, where we observe each peptide showing increased restriction once GUVs were added. Additionally circular dichroism spectroscopy (CD) measurements were taken for each analogue with and without GUV to confirm no major changes in structure on adding MTSL spin label.

Although observing morphological changes induced by this peptide gives us some insight into its mechanism of action, questions like “how physicochemical characteristics, secondary structure and charge, affect the system?” still need to be investigated. To achieve this, we chemically modified the peptide systematically to understand the structure-function relationship of mentioned physicochemical properties.

3.5 Peptide modifications and their effects on activity

Do electrostatics and secondary structure play a role in facilitating the observed peptide-membrane interaction? To address this question, we altered the OBOC screened peptide in

two limiting ways (Figure 5a). First, we dimerized the LBF14 peptide via N- to N-terminus and C- to C-terminus cysteine-mediated disulfide linkage. We named these two peptides [c-LBF14]$_2$ (dim this vastly unexplored class of erized at N-terminus) and [LBF14-c]$_2$ (dimerized at C-terminus). Our rationale is that dimeric peptides might acquire a more stable secondary structure and hence more membrane active. Second, we replaced positively charged amino acid side-chains (i.e., arginine and lysine) with an acetylated lysine, in order to mute all positive charges on the peptide side-chains while keeping the N-terminus amine free. This modified peptide, referred to as LBF14[Ac], permits investigation into the importance of cationic residues for membrane activity[33,34]. To characterize peptide-mediated membrane disruptions, we investigated the morphological changes of fungal GUVs induced by each modified peptide at the same concentration range as the unmodified peptide (1 μM to 200 μM) (Figure 5b). As expected, the higher the peptide concentration, the more pronounced the effects were, yet notably, all peptides showed various kinetics. For example, with LBF14[Ac] peptide, more vesicles were able to reach the stage of bursting at the same concentration as LBF14, suggesting that LBF14[Ac] exhibits more potent membrane activity (Figure 5b).

Using circular dichroism (CD) spectroscopy, we determined that LBF14 exists primarily as random coil without any secondary structure, whether GUVs are present or not (Figure 6). This finding is quite different from many other known MAPs, which often adapt an α-helical structure, if not already α-helical, when interacting with membrane[33,35]. As shown in Figure 6, [c-LBF14]$_2$ and [LBF14-c]$_2$ contain a substantial faction of α-helical character, although [LBF14-c]$_2$ includes a significant amount of random coil as well. The CD spectra of both [c-LBF14]$_2$ and [LBF14-c]$_2$ peptide dimers remain unaffected in the presence of membranes. In contrast, the acetylated peptide LBF14[Ac] monomer showed primarily random coil structure in the presence or absence of membranes, similar to that of the LBF14-parent peptide. Calculations for the fraction of secondary structure from the spectral fits are presented in SI Section S1.4 Table 1. Several algorithms have been developed to estimate secondary structural content in polypeptides, and the predictions vary depending on the model and parametric weighting[36,37]. Although uncertainty in the absolute values of calculated populations is inherent to each prediction method, the goodness of fit provides confidence in quantifying differences in secondary content within experimental groups. For the purpose of this study, the high signal:noise of the data and low RSMD of the fits (<0.3 in all cases) allows us to identify significant differences in secondary structure among our samples

4. DISCUSSION

A unifying feature for MAPs is their amphipathicity with different degrees of cationicity and hydrophobicity, possibly contributing to their membrane activity[38,39,40]. Some of the most intensely studied MAPs are ones that exhibit a primarily a-helical structure, either in solution or upon interacting with a membranous environment, as this might provide them with a continuous hydrophobic surface[1,41]. The repertoire of peptides - synthetic and natural - that do not adopt this or any well-defined structure has been comparatively limited. Here, we have found a completely novel, synthetic peptide containing unnatural amino acids, that interacts with different types of membrane, irrespective of its charge and secondary structure

and have systematically studied its local, mechanistic interaction with a biomembrane. This peptide cleanly falls into the category recently described as peptides displaying “interfacial activity”[8,21]. Interfacial peptides are of great interest as they not only interact with membrane lipids but also employ delocalized, allosteric behaviors, that can be identified using our strategy of sequentially screening of a random and diverse OBOC combinatorial peptide library, based on initial membrane-binding. This tool of discovery may be extremely important in investigating this vastly unexplored class of peptides, while expanding our knowledge base of how MAPs function.

Historically, interaction of biomembranes with peptides is interpreted using a one-to-one interaction model, which is typically expressed in terms of peptides causing disturbed packing in the lipids with which they interact. Peptides have also been described to demonstrate “interfacial activity,” which indicates a singular peptide interacting with lipid headgroups in a rather disorganized yet localized manner. Could it be that instead, a number of peptides bind to the membrane, driving a morphological mesoscopic global deformation event which may be a determinant of membrane activity? We describe that the critical level at which peptide effects the membrane is not local, but rather global, and describe the nature of this disturbance and its profound consequences on the level of global morphology.

Membrane activity is often manifested as pore formation or a similar mechanism that are all essentially a form of local, peptide/lipid interaction, forming as a direct consequence of peptide location and orientation - which is often dependent on secondary structure. Tubes, however, may form due to allosteric effect of peptides lodged in the membrane as demonstrated in our system. Thus our observed tube formation may represent a deviation from the classical membrane activity mechanisms.

Interfacial activity, first posited by Wimley and colleagues[21], describes the interaction of a singular peptide with a specific region of the bilayer called the interfacial zone - a 10–15 angstrom interface where polar head-groups, solution counterions, and water co-exist. They suggest that this interfacial partitioning of the peptide perturbs local lipid packing normal to the membrane bilayer, which in turn disturbs the normally strict segregation of polar and hydrophobic residues locally. Our results suggest an alternate mode of interfacial activity and membrane deformation. Here, peptide insertion into the outer leaflet of membrane bilayers gives rise to gross and delocalized morphological remodeling, which lead to topological transformation and compromise membrane stability and impermeability.

Our OBOC-borne, structurally and chemically unique peptide, that has demonstrated this dramatic global change and exhibits promiscuous membrane activity, is investigated for its mechanism of action to understand on a molecular level; how it enables the dramatic deformation of the membrane into tangles. We have shown that the observed tubulations correlated directly with MAP concentration; at the highest concentration, the major effect observed was disintegration of GUVs into a dense tangle of tubules. We propose here that several copies of LBF14, above a minimum threshold concentration, collectively lodge themselves in the outer leaflet of the bilayer as confirmed by EPR spectra, and allosterically cause a difference in lipid bilayer packing and generation of long tubules. We use this to advance the notion that the field of MAPs focuses on localized deformation of a single

peptide on a membrane - as seen time and again in simulation/docking studies or proposed mechanisms like barrel-stave, carpet model - in the form of local perturbation and packing where a peptide inserts. We propose a new notion that the ability of a peptide to induce membrane activity may not be related to a local perturbation but a delocalized morphological restructuring occurring at a much larger scale, consistent with the scale of the microorganism that is being attacked i.e. the membrane. OBOC is a robust technique for exploring this field further because the bead is coated with millions of copies of the same peptide so our search algorithm already incorporates a multi-peptide attack on the membrane.

What constitutes membrane activity? A single MAP presented to the membrane may not affect any change whereas a small local concentration might induce localized pore formation which still may not be classified as effectively membrane active. A significant determinant of membrane activity may not be a sequestered effect but a delocalized morphological shift which opens up the discovery of new MAPs that may not be classified based on physicochemical characteristics like alpha helicity, which is tied extensively to effective localized mechanisms. Our discovered lead MAP fits this exact characteristic which lead us to believe that the search for MAPs should be expanded to a broader repertoire where peptides inherently destabilized not just local but non-local conformational behaviors of the membrane, which can be facilitated by a powerful combinatorial technique like OBOC as demonstrated.

5. CONCLUSION

Through a process of systematic sequential screening, identification, and confirmation of our lead peptide LBF14, we have established an effective method to discover new MAPs on the basis of initial membrane binding. This method can be fine-tuned to discover peptides specific to a desired membrane composition. This technique also allowed us to discover a lead peptide, agnostic of current physicochemical characteristics that stratify types of membrane activity, which exhibits membrane activity by inducing mesoscopic morphological deformations in an anisotropic, allosteric fashion, and can be modelled to further explore previously undetected MAPs with similar activity.

Further, we probed the molecular milieu of peptides and characterized its membrane-deforming effect by combining real-time spinning disc confocal microscopy with electron paramagnetic resonance to reveal that local interfacial activity exhibited by LBF14 induces global morphological remodeling of the membrane into tangles of tubules, as opposed to formation of an organized local membrane structure (e.g. well-defined pores).

This discovery and characterization technique may help exploration of a class of short, synthetic MAPs containing unnatural amino acids to potentially improve their in vivo half-life, and therefore may confer clinical utility as antimicrobial peptides. Work is currently underway to use this technique to explore the arena of more selective antifungal peptides as well as exploration of biophysical characteristics of other lead peptides. We believe that this technique has the potential to generate highly-potent but previously unknown motifs that

may be important in the fields of drug delivery across cell membranes and anti-microbial drug discovery.

Supplementary Material

Refer to Web version on PubMed Central for supplementary material.

ACKNOWLEDGMENT

This work was supported in part by NIH/NCI Grants (R01CA115483, U01CA198880, and NIH/NIBIB Grant (R01EB012569) awarded to K.S.L. Edman Degradation is supported by UC Davis Comprehensive Cancer Center Support Grant (CCSG) awarded by National Cancer Institute (NCI P30CA093373).

Funding Sources

No competing financial interests have been declared.

Abbreviations

MAPs	Membrane Active peptides
OBOC	One-bead-one-compound
GUVs	Giant Unilamellar Vesicles
CPP	Cell-Penetrating Peptide
EPR	Electron Paramagnetic Resonance
CD	Circular Dichroism

REFERENCES

(1). Zasloff M Antimicrobial Peptides of Multicellular Organisms. Nature 2002, 415 (6870), 389–395. [PubMed: 11807545]

(2). Hoffmann JA Phylogenetic Perspectives in Innate Immunity. Science 1999, 284 (5418), 1313–1318. 10.1126/science.284.5418.1313. [PubMed: 10334979]

(3). Shai Y Mode of Action of Membrane Active Antimicrobial Peptides. Biopolymers 2002, 66 (4), 236–248. 10.1002/bip.10260. [PubMed: 12491537]

(4). Mishra B; Reiling S; Zarena D; Wang G Host Defense Antimicrobial Peptides as Antibiotics: Design and Application Strategies. Current Opinion in Chemical Biology 2017, 38, 87–96. [PubMed: 28399505]

(5). Heitz F; Morris MC; Divita G Twenty Years of Cell-Penetrating Peptides: From Molecular Mechanisms to Therapeutics. British journal of pharmacology 2009, 157 (2), 195–206. [PubMed: 19309362]

(6). Kauffman WB; Fuselier T; He J; Wimley WC Mechanism Matters: A Taxonomy of Cell Penetrating Peptides. Trends Biochem. Sci. 2015, 40 (12), 749–764. 10.1016/j.tibs.2015.10.004. [PubMed: 26545486]

(7). Carney RP; Thillier Y; Kiss Z; Sahabi A; Heleno Campos JC; Knudson A; Liu R; Olivos D; Saunders M; Tian L; Lam KS Combinatorial Library Screening with Liposomes for Discovery of Membrane Active Peptides. ACS combinatorial science 2017, 19 (5), 299–307. [PubMed: 28378995]

(8). Rathinakumar R; Walkenhorst WF; Wimley WC Broad-Spectrum Antimicrobial Peptides by Rational Combinatorial Design and High-Throughput Screening: The Importance of Interfacial

Activity. Journal of the American Chemical Society 2009, 131 (22), 7609–7617. [PubMed: 19445503]

(9). Rhee M; Davis P Mechanism of Uptake of C105Y, a Novel Cell-Penetrating Peptide. J. Biol. Chem. 2006, 281 (2), 1233–1240. 10.1074/jbc.M509813200. [PubMed: 16272160]

(10). de Coupade C; Fittipaldi A; Chagnas V; Michel M; Carlier S; Tasciotti E; Darmon A; Ravel D; Kearsey J; Giacca M; Cailler F Novel Human-Derived Cell-Penetrating Peptides for Specific Subcellular Delivery of Therapeutic Biomolecules. Biochemical Journal 2005, 390 (2), 407–418 90 (2), 407–418 [PubMed: 15859953]

(11). Futaki S; Suzuki T; Ohashi W; Yagami T; Tanaka S; Ueda K; Sugiura Y Arginine-Rich Peptides. An Abundant Source of Membrane-Permeable Peptides Having Potential as Carriers for Intracellular Protein Delivery. J. Biol. Chem. 2001, 276 (8), 5836–5840. 10.1074/jbc.M007540200. [PubMed: 11084031]

(12). Wender PA; Mitchell DJ; Pattabiraman K; Pelkey ET; Steinman L; Rothbard JB The Design, Synthesis, and Evaluation of Molecules That Enable or Enhance Cellular Uptake: Peptoid Molecular Transporters. Proc. Natl. Acad. Sci. U.S.A. 2000, 97 (24), 13003–13008. 10.1073/pnas.97.24.13003. [PubMed: 11087855]

(13). Lau JL; Dunn MK Therapeutic Peptides: Historical Perspectives, Current Development Trends, and Future Directions. Bioorganic & Medicinal Chemistry 2018, 26 (10), 2700–2707. [PubMed: 28720325]

(14). Koren E; Torchilin VP Cell-Penetrating Peptides: Breaking through to the Other Side. Trends in Molecular Medicine 2012, 18 (7), 385–393. [PubMed: 22682515]

(15). Milletti F Cell-Penetrating Peptides: Classes, Origin, and Current Landscape. Drug Discovery Today 2012, 17 (1516), 694–704.

(16). Avci FG; Akbulut BS; Ozkirimli E Membrane Active Peptides and Their Biophysical Characterization. Biomolecules 2018, 8 (3), 77–43.

(17). Wang G; Li X; Wang Z APD2: The Updated Antimicrobial Peptide Database and Its Application in Peptide Design. Nucleic Acids Res 2009, 37 (Database issue), D933–D937. 10.1093/nar/gkn823. [PubMed: 18957441]

(18). Perron GG; Zasloff M; Bell G Experimental Evolution of Resistance to an Antimicrobial Peptide. Proc. Biol. Sci. 2006, 273 (1583), 251–256. 10.1098/rspb.2005.3301. [PubMed: 16555795]

(19). Fjell CD; Hiss JA; Hancock REW; Schneider G Designing Antimicrobial Peptides: Form Follows Function. Nature Reviews Drug Discovery 2011, 11 (1), 37–51. [PubMed: 22173434]

(20). Lee EY; Wong GCL; Ferguson AL Machine Learning-Enabled Discovery and Design of Membrane-Active Peptides. Bioorganic & Medicinal Chemistry 2018, 26 (10), 2708–2718. [PubMed: 28728899]

(21). Wimley WC Describing the Mechanism of Antimicrobial Peptide Action with the Interfacial Activity Model. ACS Chemical Biology 2010, 5 (10), 905–917. [PubMed: 20698568]

(22). Moravej H; Moravej Z; Yazdanparast M; Heiat M; Mirhosseini A; Moosazadeh Moghaddam M; Mirnejad R Antimicrobial Peptides: Features, Action, and Their Resistance Mechanisms in Bacteria. Microbial drug resistance (Larchmont, N.Y.) 2018, 24 (6), 747–767.

(23). Lam KS; Salmon SE; Hersh EM; Hruby VJ; Kazmierski WM; Knapp RJ A New Type of Synthetic Peptide Library for Identifying Ligand-Binding Activity. Nature 1991, 354 (6348), 82–84. [PubMed: 1944576]

(24). Lam KS; Lebl M; Krchnâk V The “One-Bead-One-Compound” Combinatorial Library Method. Chemical Reviews 1997, 97 (2), 411–448. [PubMed: 11848877]

(25). Moore S; Stein WH Photometric Ninhydrin Method for Use in the Chromatography of Amino Acids. J. Biol. Chem. 1948, 176 (1), 367–388. [PubMed: 18886175]

(26). Ellman GL Tissue Sulfhydryl Groups. Archives of Biochemistry and Biophysics 1959, 82 (1), 70–77. 10.1016/0003-9861(59)90090-6. [PubMed: 13650640]

(27). Angelova MI; Dimitrov DS Liposome Electroformation. Faraday Discuss. Chem. Soc. 1986, 81 (0), 303–311. 10.1039/DC9868100303.

(28). Su W-C; Gettel DL; Chabanon M; Rangamani P; Parikh AN Pulsatile Gating of Giant Vesicles Containing Macromolecular Crowding Agents Induced by Colligative Nonideality. J. Am. Chem. Soc. 2018, 140 (2), 691–699. 10.1021/jacs.7b10192. [PubMed: 29303581]

(29). Collins MD; Gordon SE Giant Liposome Preparation for Imaging and Patch-Clamp Electrophysiology. JoVE 2013, No. 76, 50227 10.3791/50227.

(30). Joon Oh K; Altenbach C; Collier RJ; Hubbell WL Slte-DlrecteU Spin Labeling of Proteins. Bacterial Toxins: Methods and Protocols; Holst, O., EU.; Methods in Molecular Biology™ Humana Press: Totowa, NJ, 2000; pp 147–169. https://Uoi.org/10.1385/1-59259-052-7:147.

(31). Bestsel http://bestsel.elte.hu/inUex.php (accessed Oct 22, 2019).

(32). van Meer G; Ue Kroon AIPM. LipiU Map of the Mammalian Cell. Journal of Cell Science 2010,

(33). EpanU RM; Vogel HJ Diversity of Antimicrobial Peptides anU Their Mechanisms of Action. Biochim. Biophys. Acta 1999, 1462 (1–2), 11–28. https://Uoi.org/10.1016/s0005-2736(99)00198-4. [PubMed: 10590300]

(34). Hoernke M; Schwieger C; Kerth A; Blume A BinUing of Cationic PentapeptiUes with MoUifieU SiUe Chain Lengths to Negatively ChargeU LipiU Membranes: Complex interplay of Electrostatic anU HyUrophobic interactions. Biochim. Biophys. Acta 2012, 1818 (7), 1663–1672. https://Uoi.org/10.1016/j.bbamem.2012.03.001. [PubMed: 22433675]

(35). Tang H; Yin L; Kim KH; Cheng J Helical Poly(Arginine) Mimics with Superior Cell-Penetrating anU Molecular Transporting Properties. Chem Sci 2013, 4 (10), 3839–3844. https://Uoi.org/10.1039/C3SC51328A. [PubMed: 25400902]

(36). Greenfield NJ Using Circular Dichroism Spectra to Estimate Protein Secondary Structure. Nat Protoc 2000, 1 (6), 2876–2890. 10.1038/nprot.2006.202.

(37). Micsonai A; Wien F; Kernya L; Lee Y-H; Goto Y; Réfrégiers M; Kardos J Accurate Secondary Structure Prediction and Fold Recognition for Circular Dichroism Spectroscopy. Proc Natl Acad Sci USA 2015, 112 (24), E3095–E3103. 10.1073/pnas.1500851112. [PubMed: 26038575]

(38). Lohner K New Strategies for Novel Antibiotics: Peptides Targeting Bacterial Cell Membranes. Gen. Physiol. Biophys. 2009, 28 (2), 105–116. 10.4149/gpb_2009_02_105.

(39). Bradshaw J Cationic Antimicrobial Peptides : Issues for Potential Clinical Use. BioDrugs 2003, 17 (4), 233–240. 10.2165/00063030-200317040-00002. [PubMed: 12899640]

(40). Nguyen LT; Haney EF; Vogel HJ The Expanding Scope of Antimicrobial Peptide Structures and Their Modes of Action. Trends in Biotechnology 2011, 29 (9), 464–472. 10.1016/j.tibtech.2011.05.001. [PubMed: 21680034]

(41). Takahashi D; Shukla SK; Prakash O; Zhang G Structural Determinants of Host Defense Peptides for Antimicrobial Activity and Target Cell Selectivity. Biochimie 2010, 92 (9), 1236–1241. 10.1016/j.biochi.2010.02.023. [PubMed: 20188791]

HIGHLIGHTS

- Discovery of new membrane active peptide, LBF14, by screening a 100,000-member OBOC library to search for initial biomembrane binding as a marker of membrane activity
- LBF14 shows no homology with current MAPs and doesn't conform to physicochemical "rules" established for MAPs.
- LBF14 induces gross morphological disruption of membranes, irrespective of membrane composition as observed by spinning disc confocal microscopy in real time.
- EPR studies further demonstrated that LBF14 is adsorbed on the membrane then buried itself into the outer leaflet anchored to the outer bilayer.
- Discovery of LBF14 through unbiased library screening for membrane binding is an important tool for exploring new MAPs displaying activity by local insertion and subsequent membrane disruption

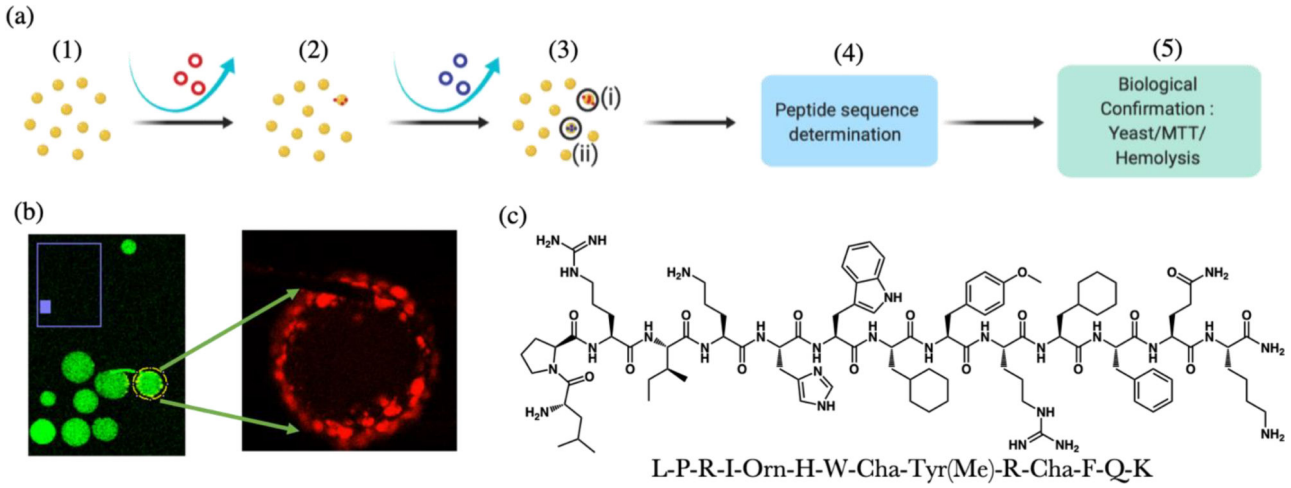

Figure 1.

(a) Scheme of sequential screening strategy with two different GUVs to detect MAP from OBOC combinatorial peptide library: Step 1 - Incubate immobilized beads with “fungal GUVs” (in red), then wash away non-binding ones. Step 2 - Identify positive-binding hits with GUVs visibly bound to the bead, record position and remove bound GUVs by washing with ethanol. Incubate immobilized beads with “mammalian GUVs” (in blue), then wash away non-binding ones and identify positive-binding hits. Step 3 - Identify and isolate positive beads of interest; ‘(i)’ depicts peptide bead that bound both types of membranes (non-specific binding) while ‘(ii)’ depicts peptide bead that bound fungal-GUVs selectively (fungal-specific binding). Step 4 - Selected beads microsequenced via automatic Edman chemistry[7]. Step 5 - To confirm membrane activity in relevant biological systems, lead compounds resynthesized in soluble form and their biological effects on yeast, HEK 293 kidney cells, and red blood cells determined. (b) Visual representation of bead-bound LBF14 lead peptide. Beads auto-fluoresce in GFP channel (488nm) but not in the rhodamine channel (550nm). This has enabled us to clearly visualize rhodamine-DOPE labelled GUVs which uniformly bind to the bead surface even after unbound/weakly bound GUVs were washed away. (c) Primary structure of LBF14.

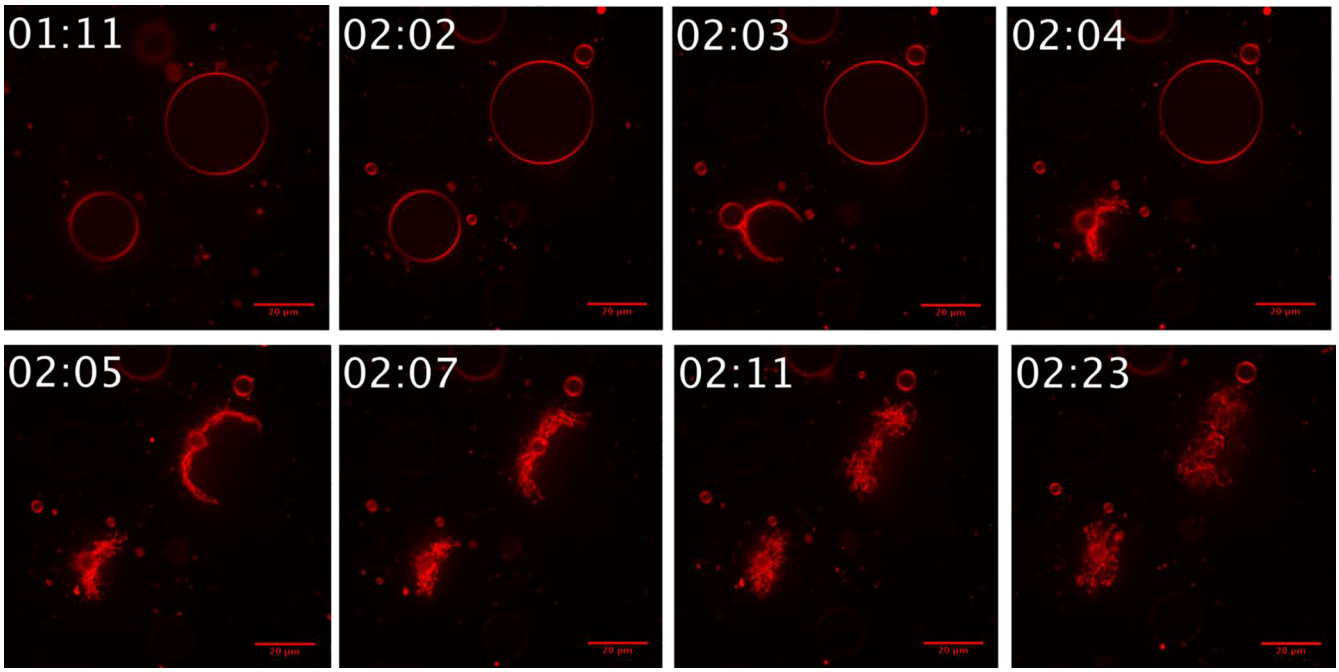

Figure 2.

Fast dynamics of GUV bursting into tubular networks, under high concentration of MAP, captured by spinning disc confocal microscopy (See SI video S2.1). Each frame was time-stamped, with time zero representing the addition of GUVs (2 μL of GUV solution) into a 200 μL solution of 100 μM LBF14 peptide. Short tubules/budding emerging from the membrane were observed. As time passes, this effect was more pronounced as seen in 2.02 min snapshot around both vesicles. At 2.03 min, the GUV at the left lower quadrant burst open and reorganized itself into a tangle of tubular structures, as the GUV at the right upper quadrant underwent the same process at 2.05 min. This interaction was found to be very dynamic as shown, where within a second the topography of membrane completely changed. Scale bar is 20 μm. The actual movie of this figure is shown in (See SI video S2.1).

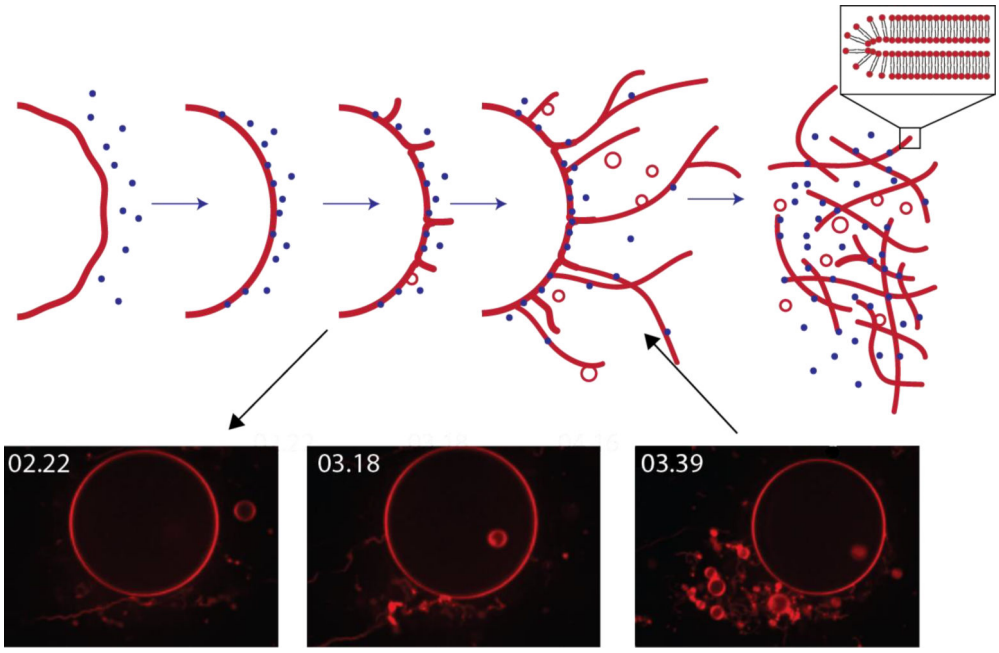

Figure 3.

Proposed model for the journey of the membrane of a GUV during LBF14 peptide insertion, presented as biophysical phenomena. An initially floppy membrane is exposed to peptide that start to insert at the membrane interface. This activity causes the membrane to assume a tighter, more rigid structure due to peptide burying and resultant molecular crowding. Eventually, crowding leads to a breaking point where the asymmetry in area between the outer and inner bilayer leaflets cannot be sustained, and the membrane begins to pinch off as tubular or bud-like structures. As an increasing number of peptides are adsorbed into the membrane, this effect presents as increasingly aggressive, generating even more mesoscopic deformations and small membrane vesicle formation. At this point the membrane rapidly disrupts and reorganizes into a network of tubular structures, likely stabilized by the peptide. Snapshots at 2.22, 3.18 and 4.16 min (LBF14 at 25 μM with Fungal GUV, See SI video S2.3) are given to illustrate how the tabulation effect graduates from mere pinching off to aggressive lipid displacement in the form of a tangle of tubes which eventually causes GUV bursting. Top right corner represents the cross section of these tubules.

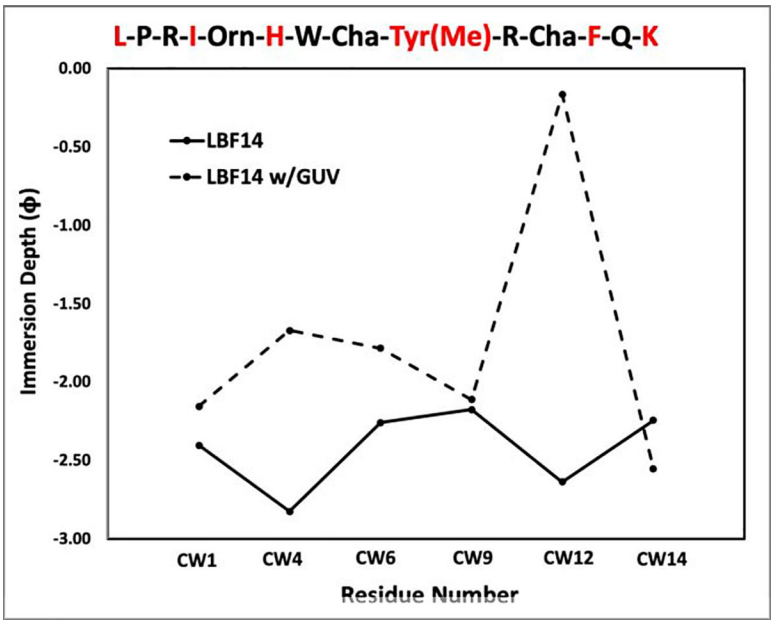

Figure 4.

Immersion Depth parameter (∅) of LBF14 into the membrane. Electron paramagnetic resonance studies of spinlabeled LBF14 MAP. EPR power saturation series for Cysteine-Walk analogues (See SI section S1.3 Figure 4) of LBF14 peptide before (solid line) and after (dotted line) addition of Fungal GUVs. Higher value of immersion depth parameter is indicative of a more hydrophobic environment, in other words, is deeply buried in the membrane. Upon addition of membrane vesicles, some positions like CW4, CW6 and CW12 became increasingly restricted or deeply buried in the membrane. Residues shown in red were replaced one by one to generate analogues shown in SI.

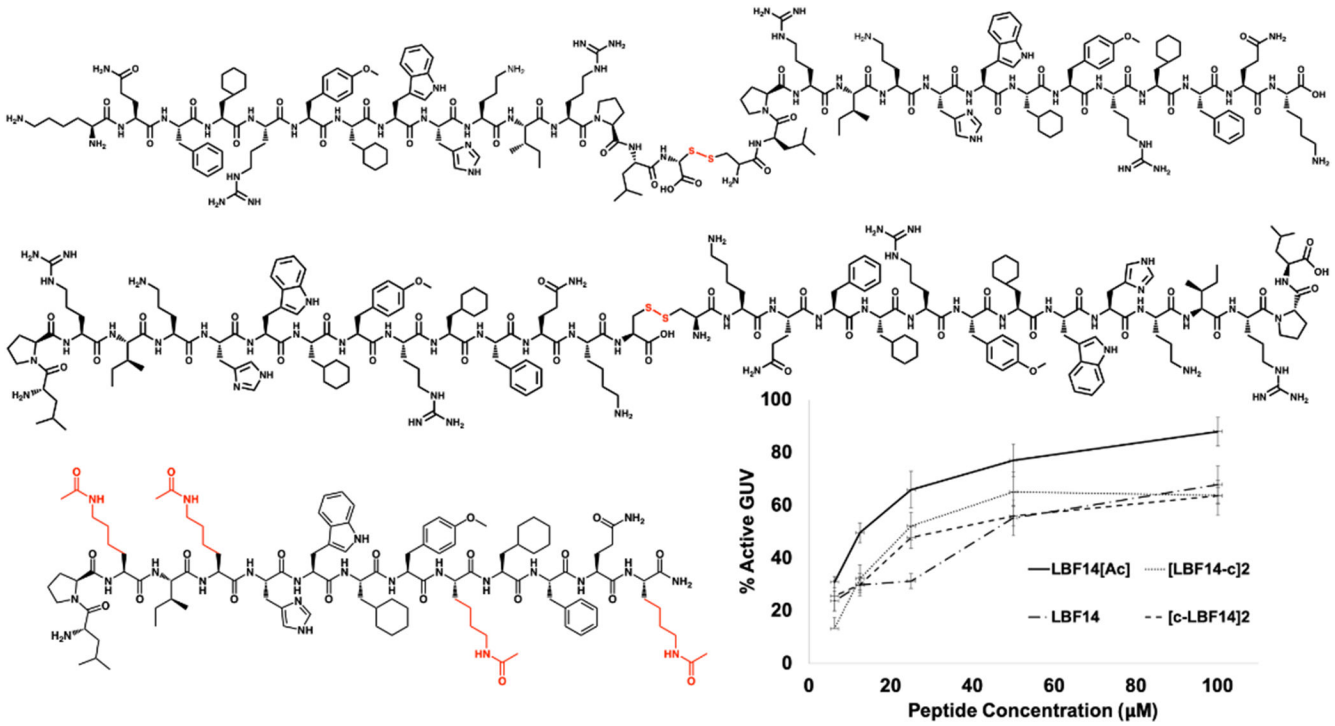

Figure 5.

Membrane activity of LBF14 and its derivatives. (a) Chemical modifications were performed on LBF14 peptide, including addition of cysteine to either the N-terminus or C-terminus (top structure vs. middle structure) to induce peptide homo-dimerization via disulfide linkage to form $[c\text{-LBF14}]_2$ (dimerized at N-terminus) and $[LBF14\text{-}c]_2$ (dimerized at C-terminus). In a separate experiment, all positively charged amino acid side chains were replaced with acetylated lysine (LBF14[Ac], lower structure) to examine the contribution of the cationic residues to membrane activity. (b) Membrane activity, as measured by the % “active vesicles” as a function of peptide concentration. Acetylated LBF14 was found to be more membrane active than the other three peptides, at all concentration levels. Dimerization did not significantly affect its potency.

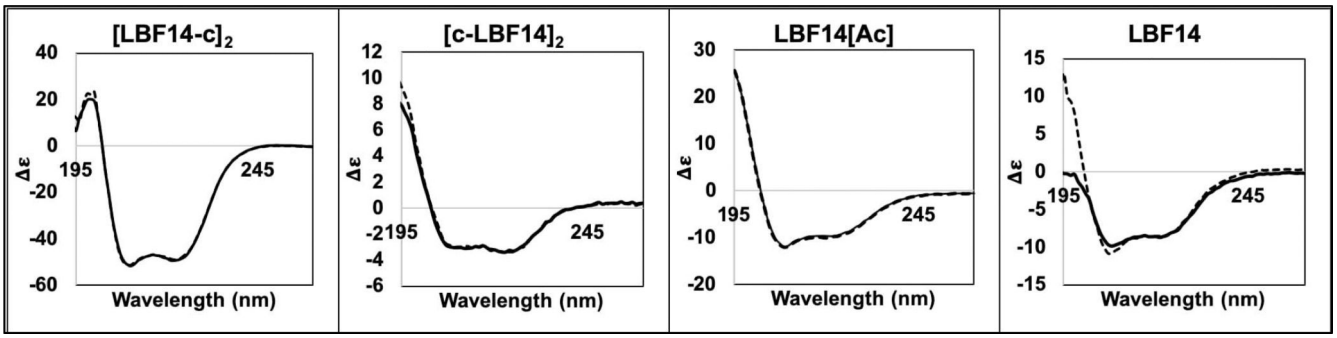

Figure 6.

Circular dichroism (CD) results for modified peptides $[LBF14\text{-}c]_2$, $[c\text{-}LBF14]_2$ and LBF14[Ac] compared with LBF14 parent peptide with and without GUVs. No sign of α-helical secondary structure was detected in $[c\text{-}LBF14]_2$, LBF14[Ac], or LBF14, even with addition of GUVs. Instead, these three peptides displayed 55–65% random coil character as determined by fitting curves (See SI Section S1.4 Table 1). $[LBF14\text{-}c]_2$, on the other hand, presented primarily as 43% and 50% α-helical structure, with and without addition of GUV, respectively.

Table 1.

List of Amino acids used as the OBOC combinatorial library as building blocks.

	Amino Acid		Amino Acid
1	*Nα-Fmoc-Arg(Pmc)-OH*	13	*Nα-Fmoc-Phe-OH*
2	*Nα-Fmoc-Asn(Trt)-OH*	14	*Nα-Fmoc-Pro-OH*
3	*Nα-Fmoc-Asp(OtBu)-OH*	15	*Nα-Fmoc-Val-OH*
4	*Nα-Fmoc-Gln(Trt)-OH*	16	*Nα-Fmoc-Hyp-OH*
5	*Nα-Fmoc-glu(OtBu)-OH*	17	*Nα-Fmoc-Aib-OH*
6	*Nα-Fmoc-His(Trt)-OH*	18	*Nα-Fmoc-Nva-OH*
7	*Nα-Fmoc-Lys(Boc)-OH*	19	*Nα-Fmoc-Dpr-OH*
8	*Nα-Fmoc-Trp(Boc)-OH*	20	*Nα-Fmoc-Tyr(Me)-OH*
9	*Nα-Fmoc-Ala-OH*	21	*Nα-Fmoc-Nle-OH*
10	*Nα-Fmoc-Gly-OH*	22	*Nα-Fmoc-Cha-OH*
11	*Nα-Fmoc-Ile-OH*	23	*Nα-Fmoc-Om(Boc)-OH*
12	*Nα-Fmoc-Leu-OH*	24	*Nα-Fmoc-Abu-OH*